RESEARCH ARTICLE | NOVEMBER 05 2024

Scaling transition of turbulent flame speed for thermodiffusively unstable flames

Guido Troiani ; Pasquale Eduardo Lapenna ; Francesco D'Alessio ; Francesco Creta

Physics of Fluids 36, 115122 (2024)
https://doi.org/10.1063/5.0232458

Physics of Fluids ARTICLE pubs.aip.org/aip/pof

Scaling transition of turbulent flame speed for thermodiffusively unstable flames

Cite as: Phys. Fluids **36**, 115122 (2024); doi: 10.1063/5.0232458
Submitted: 7 August 2024 · Accepted: 11 October 2024 ·
Published Online: 5 November 2024

Guido Troiani,[1,a)] Pasquale Eduardo Lapenna,[2] Francesco D'Alessio,[2] and Francesco Creta[2]

AFFILIATIONS

[1]Laboratory of Sustainable Combustion and Thermal & Thermodynamic Cycles, ENEA C.R. Casaccia, Rome, Italy
[2]Department of Mechanical and Aerospace Engineering, Sapienza University of Rome, Rome, Italy

[a)]Author to whom correspondence should be addressed: guido.troiani@enea.it

ABSTRACT

This work presents an experimental set of Bunsen flames characterized by a moderate Reynolds number and a variable turbulence intensity. Ten lean hydrogen-enriched methane–air mixtures at three turbulence levels are investigated, ranging from methane–air to hydrogen–air mixtures. Such mixtures are selected to have an almost constant laminar flame speed while inducing the onset of thermal-diffusive (TD) instability by gradually increasing the hydrogen content of the blend. The flames' global consumption speed, stretch factor, and flame surface area are investigated and discussed as functions of the effective Lewis number of the mixture. As the interplay between TD instability and turbulence enhances the overall flame propagation, below a transitional Lewis number, flames are observed to be particularly sensitive to external turbulent forcing. This synergistic interaction is discussed in terms of Karlovitz and Lewis numbers. A parameterization of the turbulent flame speed is thus proposed, based on a functional form depending, concurrently, on both Karlovitz and Lewis numbers. The proposed form is shown to fit the experimental results at different turbulence levels and to capture the flame speed enhancement across the transitional Lewis number.

I. INTRODUCTION

In the context of turbulent premixed combustion, the turbulent flame speed S_T is defined as the speed at which reactants are consumed through a suitably defined average flame surface. It is one of the fundamental quantities to investigate and characterize to model premixed flames in a turbulent setting. An initial attempt to parameterize this quantity dates back to the seminal work of Damkhöler,[1] and the search for a model of the turbulent flame speed has been relentless ever since.[2–6]

For carbon-based fuels, where thermal and mass diffusivities can generally be of the same order at near-stoichiometric conditions, the dependence of turbulent flame speed is sought in terms of observables that can affect the amount of flame wrinkling, such as the whole spectrum of turbulent kinetic energy and its dissipation rate, usually expressed in terms of the turbulent velocity fluctuations as well as external and Taylor scales. The flame thermochemical parameters also play their role: namely thermal expansion, thermal thickness, laminar flame speed, whether strained (S_L) or unstrained (S_L^0). Usually, such quantities are used in non-dimensional form, i.e., the turbulent velocity fluctuations in units of laminar flame speed u'/S_L, thermal thickness in units of integral length scale L_T/ℓ_0, the Schmidt or Zel'dovich numbers as well as the Markstein number. In this context, much work was done to model the experimental measurements of the turbulent flame speed.[7–11]

Following a slightly different approach, attempts were also made to decouple the effects of the turbulent area A_T from the diffusive effects acting within the flame front thickness. To this end, the turbulent flame speed was modeled as $S_T/S_L^0 \sim I_0(A_T/A_0)$, where A_0 is the unwrinkled mean flame area and the stretching factor I_0 is a measure of the discrepancy between the increase in turbulent flame speed and the increase in turbulent area,[12–15] effectively accounting for the variation of flame reactivity due to turbulence. An interesting scaling for I_0 with the Karlovitz number was proposed in Ref. 16, $I_0 \sim Ka^{(1/3)}$, which well fits the experimental results of Refs. 17 and 18 in which, again, the fuel Lewis number is kept close to one.

An additional effect to be taken into account is the onset of the intrinsic hydrodynamic or Darrieus–Landau (DL) instability, which can potentially affect propagation at large scales. Asymptotic theory and, more recently, direct numerical simulations (DNSs)[19–23] have been used to perform linear stability analyses for premixed flames

yielding dispersion relations for the growth rate of harmonic flame disturbances. A cutoff length scale λ_c emerges so that any disturbance larger than this is exponentially amplified in the linear regime. In practical situations, when the integral scale of the system is larger than the cutoff scale, the flame can exhibit a range of unstable scales that further enhance the wrinkling,[24–27] although at higher turbulence intensity a unified turbulence-dominated regime is likely reached.[15,28,29]

The use of hydrogenated carbon-based fuels to mitigate carbon dioxide emissions introduced the additional effect of uneven heat and fuel mass diffusivities, resulting in Lewis numbers potentially significantly smaller than unity. This leads to the activation of an additional intrinsic instability mechanism, of thermodiffusive (TD) nature and active at smaller scales, which has been observed, both numerically and experimentally, to deeply affect both laminar and turbulent flame propagation, in particular when the Lewis number is lowered below a critical transitional value.[6,22,30–33] As an exemplification of the differences between TD-stable/TD-unstable flames, Fig. 1 shows OH-LIF measurements performed by the authors, used to trace the reactivity and morphology of lean methane–air and hydrogen–air Bunsen flames. On one hand, DL (pure methane) instabilities, which introduce a distinct cellularity in the flame conformation, play a distinct role in increasing the turbulent area. On the other (pure hydrogen), the TD-induced stretch patterns locally increase the reaction rate, affecting the flame reactivity,[27,31,34] inducing a strong reduction of the reaction rate at cusp apexes (conventionally described with negative flame front curvatures), in contrast to a superadiabatic flame temperature at flame troughs where curvatures are positive. The two effects combined result in an enhanced combustion regime typical of low Lewis number flames. It is worth noting that the presence of thermal-diffusive instabilities alone is not possible. Being the hydrodynamic instability a phenomenon ubiquitous present in a flame, due to the thermal expansion through the flame front, that of the thermal-diffusive type is driven by the disparity between mass and thermal diffusivity, which can be eliminated by acting on the composition of the reactant mixture. In addition, very lean mixtures at high contents of hydrogen are shown to be characterized by a negative Markstein length Ma[35,36] with the result that negatively stretched laminar flames propagate faster than an equally stretched hydrocarbon-based flame whose Markstein length is positive.

In this work, we present results from an experimental campaign in which the addition of hydrogen in a methane–air Bunsen flame at constant bulk Reynolds number (mixtures ranging from pure methane to pure hydrogen) drives the Lewis number Le from almost unity toward lower values. Such a set of variable Le flames is forced with different levels of turbulence, achieved by moving a perforated plate along the streamwise direction. Mixtures are chosen to maintain the laminar flame speed constant while the Lewis number is decreased to isolate such effects. Then, the experimental results are presented as a function of Le and a parameterization of the turbulent flame speed is proposed to improve the existing models.

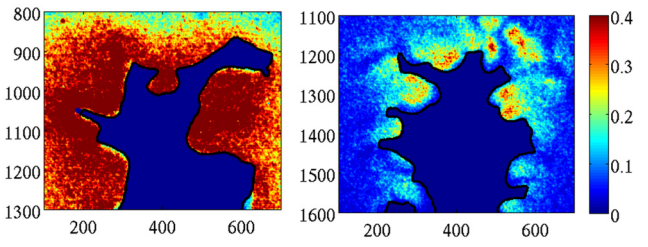

FIG. 1. OH-LIF measurements for lean methane–air flame (left panel) and lean hydrogen–air flame (right panel), as reported in Table I. LIF signal is normalized with the local maximum of each snapshot. In pure hydrogen flame, the enhancement and depletion of LIF intensity signal are visible that can be translated into an indication of the intensity of the reaction rate. Axes are reported in pixels and their resolution is about 50 μm per pixel.

In Ref. 37, asymptotic expressions show that the stretched laminar premixed flame increases its flame temperature and mass burning rate when non equidiffusion of species is present, i.e., $Le < 1$. In particular, the mass burning flux is linearly proportional to the Karlovitz number and to the inverse of the Lewis number. When the Lewis number is even lowered, thermodiffusive instability can occur, triggered by small disturbances of the flow field.[31,33] This is shown to have a deep impact on the mass burning regime and consequently on the turbulent flame speed.[6,27,31,34]

In particular, turbulent flame speed models where non-equidiffusion effects are not taken into account were proposed by authors in Refs. 8–11 with the only exception of Ref. 11 where a $Le^{0.3}$ dependence is introduced, and in Ref. 7 in which an indirect dependence from Lewis number acts through the influence on some thermochemical parameters. In a recent work,[38] this restraint was an object of attention and corrections were proposed in order to introduce explicitly the Lewis dependence. Those turbulent flame speed models, where the influence of the Lewis number is modeled with power laws having a single exponent,[11,38] do not seem to capture the behavior across the transitional Le. For this reason, in this work the parameterization proposed is based on a functional form depending on both Karlovitz and Lewis numbers, with the aim of capturing the transition across the critical Lewis number for all turbulence levels.

II. METHODS

A. Thermochemical properties

The experimental dataset features 10 different fuel–air mixtures at increasing hydrogen content, having a fuel composition that varies from pure CH_4 to pure H_2. Each condition is fully characterized by the equivalence ratio ϕ and the volumetric fraction of hydrogen α in the fuel. The (ϕ, α) combinations for the present analysis are chosen such that the unstretched laminar flame speed S_L^0 remains approximately constant, without the introduction of any bias in the turbulence–flame interaction interpretation. As the hydrogen content is increased, differential diffusion effects are expected to be more relevant. When fuel blends and realistic mixtures are considered, as in the case of hydrogenated methane–air mixtures, multiple Lewis numbers can be singled out and the definition of an effective Lewis number Le can be useful. Such effective value is evaluated using the definition of Bechtold and Matalon[35] using a single reference Lewis number for the fuel's mixture with a volume-based approach,[39]

$$Le = 1 + \frac{(Le_E - 1) + (Le_D - 1)F}{1 + F}, \tag{1}$$

where $F = 1 + Ze(\Phi - 1)$, with Ze being the Zel'dovich number and $\Phi = \phi$ the equivalence ratio, when the mixture is rich ($\phi > 1$) and $\Phi = \phi^{-1}$ for lean mixtures. Deficient and excess reactants can be either the fuel mixture under investigation or the oxygen depending

on the amount of air used, i.e., lean or rich mixture. The Lewis number of the methane and hydrogen mixture is weighted with their respective volume (or equivalently molar) fraction,

$$Le_{mixture} = (1-\alpha)Le_{CH_4} + \alpha Le_{H_2}. \quad (2)$$

Consistent with a companion work,[33] the oxidizer and fuel Lewis numbers are taken on the burned side of a laminar 1D premixed flame, simulated using Cantera[40] with detailed chemistry and transport models,[41] at each condition of interest in terms of ϕ and α. Using the same set of 1D flames, the Zel'dovich number Ze is evaluated as described in Ref. 42. The resulting Le ranges between 1.03 and 0.38 as α is increased for the 10 thermochemical conditions used in this study. The values of Le as well as the laminar unstretched flame speed S_L^0 and laminar thermal flame thickness L_T are reported in Table I. Note that, as discussed in Ref. 33, slightly different values of Le, i.e., $\pm 5\%$, can be obtained using different definitions for Ze.

A mixture is defined as thermodiffusively unstable when the effective Le is lower than a critical Le_0. Possible definitions of Le_0 stem from model dispersion relations, identifying the Lewis values that lead to a null second-order term in the dispersion relation as discussed in Ref. 30. In the present case, using realistic mixtures, we employ the model dispersion relation of Matalon *et al.*[43] as also done in recent DNS studies.[42,44] However, it is worth mentioning that the resulting Le_0 is only a qualitative indicator as the model dispersion relation can largely differ from the dispersion relations obtained using DNS.[42,45] This being said, the resulting Le_0 remains in a rather confined range between 0.50 and 0.63, confirming that the thermochemical flame conditions investigated in this work span both TD-stable (low α) and TD-unstable (high α) mixtures. Note that a detailed discussion on the stability limits of the thermochemical condition explored by the present experimental dataset is reported by the same authors in Ref. 33.

B. Turbulence characteristics and measurements

The flames investigated in this work feature a Bunsen burner configuration with a diameter of $D = 18$ mm. The same geometry and setup was employed in previous studies focusing on the interaction between DL instability and turbulence[15,24,26,29,46] at different Reynolds numbers and propane–air mixtures. For the present study, a moderate bulk Reynolds number $Re \sim 5000$ is chosen and the turbulence intensity is further modulated by a grid placed before the nozzle exit. In particular, three positions of the grid are chosen to reach different levels of axial velocity fluctuations u', located at 1D, 2.5D, and 6D from the nozzle exit. The mean axial velocity U_0, defined as the mass of fresh reactants flowing through the Bunsen cross section, is the same for the three levels of turbulent intensity, with the bulk Reynolds number being constant, thus $U_0 = 4.4$ m/s. As expected, higher u' and larger turbulence integral scale ℓ_0 are obtained when the grid is located closer to the nozzle exit as reported in Table II.

The axial velocity fluctuations are measured along the burner axis at its exit while the integral length scale is measured at the first zero crossing of the axial velocity autocorrelation coefficient along the burner axis.

The velocity fields are measured via particle image velocimetry (PIV), seeding 2 μm alumina particles in the fresh mixture as a laser sheet scans an axial plane above the Bunsen exit. Mie diffusion of light resulting from the elastic interaction between the laser light and the alumina particles is recorded by a CCD camera with a repetition rate of 10 Hz and a resolution of 2048×2048 pixels equipped with a 80 mm focal length lens and an interference filter to suppress any other wavelength of light except that at 532 nm, typical of 2^{nd} harmonic of Nd:YAG sources. The velocity field is obtained by 32×32 pixels interrogation windows with an overlap of 50%. The laser source is a 532 nm Nd:YAG delivered through a cylindrical lens to expand the beam into a laser sheet characterized by a thickness of ~ 400 μm at FWHM. The resolution for each pixel is 41 μm. The resulting images are comprised of two distinct regions defined by very different levels of scattered light intensity reflecting unburnt and burnt regions with different values of temperature and density. The steep gradient separating the two regions traces the flame front separating burnt to unburnt mixture. A threshold technique allows for the definition of a binary image, where zero values are associated with cold denser reactants and ones stand for hot burned gases, leading to the definition of a mean progress variable $\overline{C}$ ranging between 0 and 1. With binary images available, the flame front can be measured and values for the turbulent area as well as mean flame position follow.

Radical concentration measurements are performed by acquiring the fluorescence signal emitted by hydroxyl (OH) radicals. To this end, a Nd:YAG laser beam combined with a tunable dye laser and with a second-harmonic generator crystal is used to shift the laser wavelength from 532 nm down to 282.93 nm (further experimental details can be found in Ref. 47). An intensified 2048×2048 pixels SCMOS camera, triggered with PIV CCD, collects the induced fluorescence emitted at 310 nm. The fluorescence signal from OH radical is proportional to its

TABLE I. Thermochemical conditions of the experimental dataset: equivalence ratio ϕ, volumetric fraction of hydrogen in the fuel α, thermal flame thickness L_T, laminar flame speed S_L^0, and effective Lewis number Le.

Case#	ϕ (-)	α (-)	L_T (mm)	S_L^0 (m/s)	Le
1	0.875	0.0	0.48	0.33	1.03
2	0.825	0.3	0.47	0.34	0.92
3	0.775	0.3	0.49	0.32	0.85
4	0.725	0.46	0.48	0.32	0.76
5	0.675	0.6	0.48	0.33	0.67
6	0.650	0.66	0.49	0.32	0.62
7	0.625	0.72	0.49	0.32	0.59
8	0.600	0.78	0.49	0.33	0.54
9	0.550	0.88	0.49	0.33	0.47
10	0.475	1.0	0.51	0.33	0.38

TABLE II. Turbulent non-reacting flow field characterization of the Bunsen configuration at $Re \sim 5000$ for the three different grid positions resulting in *low*, *medium*, and *high* u'. Turbulence intensity, $T.U. = u'/U_0$.

Case label:	*Low*	*Medium*	*High*
Grid position	6.0 D	2.5 D	1.0 D
u' [m/s]	0.22	0.33	0.44
ℓ_0 [mm]	5.5	6.2	6.9
$T.U.$	0.05	0.075	0.1
Plots legend	○	□	△

concentration and relative measurements are possible (absolute measurements of concentrations are instead prevented from non-radiative deexcitation channels that are generally active together with detectable fluorescence emission).

Since parameters (ϕ, α) have been chosen such that S_L^0 remains approximately constant, the Karlovitz number $\mathrm{Ka} = L_T^2/\eta^2 = (u'/S_L^0)^{(3/2)}(L_T/\ell_0)^{(1/2)}$, where the Kolmogorov scale η is also approximately constant. Indeed, the location of each flame series characterized by low, medium, and high values of u' is rather close in the Borghi–Peters diagram as shown in Fig. 2.

III. RESULTS

A. Experimental turbulent flame speed

The turbulent flame speed is evaluated using the global consumption speed concept,[48]

$$S_T = \frac{\dot{m}}{\rho_u A_0}, \tag{3}$$

where $\dot{m}$ is the inlet mass flow rate of the fresh mixture of density ρ_u (at room temperature), while A_0 represents the reference surface area of the mean flame, evaluated at the averaged progress variable $\overline{C} = 0.5$, when the time-averaged flame is considered as axisymmetric. In Appendix A, implications for different values of iso $-\overline{C}$ are discussed.

Figure 3 shows the turbulent speed, normalized with the laminar unstrained speed S_L^0, as a function of Le for the three turbulent conditions investigated. Large symbols refer to the Le numbers reported in Table I, while smaller symbols, used here as a reference, represent values of Le obtained using alternative definitions, as discussed in Ref. 33 and in Sec. II A. Thus, in the figure each point of the experimental results is reported by using different values for the Lewis number to show that Lewis variations have little influence on the results discussed and that the existence as well as the identification of a transitional Lewis number is not compromised. For the lower u' case, the enhancement of S_T/S_L^0 is rather limited as the hydrogen content in the fuel blend is increased and the Lewis number is lowered. Conversely, a substantial impact of hydrogen addition can be observed for the medium u' values and even more so for the large u' cases. Comparable results are present in the literature for the corresponding thermochemical and fluid-dynamic conditions. In particular, DNS results in Ref. 38 have

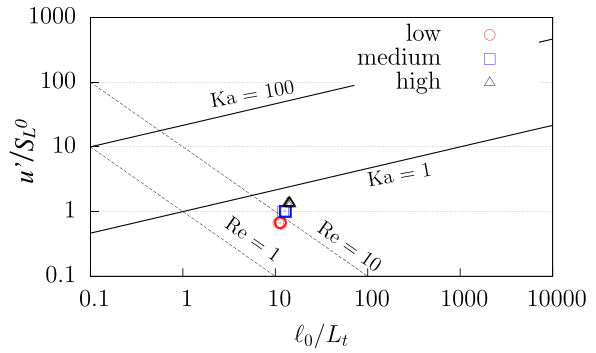

FIG. 2. Regime diagram for premixed turbulent combustion: each point represents the conditions of an experimental flame colored with the turbulence intensity that is varied through grid positioning as reported in Tables I and II.

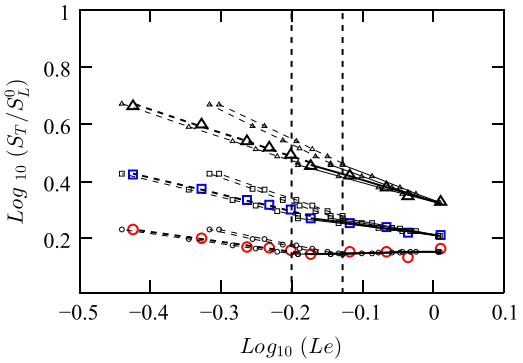

FIG. 3. Log–log plot of the turbulent flame speed S_T normalized with S_L^0. Dashed and continuous lines are linear regressions of experimental results conditioned to $Le < Le_0$ and $Le > Le_0$. For color coding, see Fig. 2. Large symbols refer to the Le numbers reported in Table I, while smaller symbols represent values of Le obtained using alternative definitions, as discussed in Ref. 33 and in Sec. II A.

comparable amplitudes of S_T for $Le = 0.34$ and $Le = 1.2$; DNS results reported in Refs. 30, 31, 49, and 50 and experiments[34,51,52] show the thermodiffusively unstable turbulent flame velocity to be almost three times larger than that of thermodiffusively stable flames. Those values are comparable to the present results, at least for the largest turbulent velocity fluctuations; DNS results reported in Ref. 22 show 65% increment of the flame velocity compared to laminar flame speed in the same thermochemical conditions.

Comparing the effect of increasing turbulence under the same thermochemical conditions, i.e., same Le, it is evident that flames with higher hydrogen content are more sensitive to increasing u'. This synergistic interaction[31] of turbulence and thermal-diffusive flame instabilities has been discussed in Ref. 33. In addition, the log–log visualization reveals not only a linear scaling but also a visibly different behavior whether the effective Lewis number is larger or smaller than a transitional value, in the range of Le_0 as previously discussed and irrespective of the turbulence levels. These limits, shown in Fig. 3 by two vertical dashed lines, encompass all the scaling transitions obtained with the different Lewis number definitions and are comprised between a minimum value and a maximum value of 0.63 and 0.74, respectively, which closely fall within the range of critical Lewis numbers $Le_0 = 0.50 - 0.63$ previously reported. It is thus reasonable to assume a reference transitional Lewis number $Le_0^* \sim 0.68$ taken as the average between the two limit values identified where the slope of S_T/S_L^0 is steepened as Le decreases. In addition, the transition between the two slopes is observed to be smoother when turbulence is increased. In other words, for flames with higher hydrogen content, the higher sensitivity to turbulence persists but the transition from thermal-diffusive unstable to stable regimes ceases to be abrupt. This behavior is akin to the unifying "turbulence-dominated regime" observed for hydrodynamically stable and unstable flames,[15,24,29] where turbulence effects in creating turbulent surface area overwhelm instability surface generation.

To further investigate the global consumption speed, we express it as

$$\frac{S_T}{S_L^0} = I_0 \frac{A_T}{A_0}, \tag{4}$$

in which two contributions are singled out: the turbulent surface area A_T, normalized with A_0, and the stretch factor I_0, which is a global measure of the deviation of the flame speed from that of an unstretched laminar flamelet. The turbulent area A_T is determined from the volume integration of the flame surface density Σ, which is the ratio between the flame surface area and its embedding volume, as discussed in Refs. 14 and 46, while the mean flame surface A_0 is defined in Eq. (3). Note that the choice of the reference surface A_0 becomes immaterial when Eq. (3) is plugged into Eq. (4).

The instantaneous flame fronts shown in Fig. 4 underline the effects of both turbulence and Lewis number on the development of the turbulent area. The increased amount of flame wrinkling acts to reduce the flame height as the turbulence is increased and the Lewis number is reduced. A quantitative visualization of the normalized turbulent area A_T/A_0, which deprives the turbulent area of flame height effects and of the influence of the mean flame, is displayed in Fig. 5 as a function of the Lewis number. Although both thermal-diffusive effects and turbulence come into play in the enhancement of the normalized turbulent area, the trend appears to have a constant slope, insensitive to the turbulence intensity and Lewis number, and no transitional behavior is observed at the critical Lewis number Le_0^*. On the other hand, if we observe the stretching factor I_0, displayed in the top panel of Fig. 6, a clear transition emerges for $Le < Le_0^*$, wherein thermal-diffusive effects act synergistically with turbulence in amplifying I_0 and thus the net flame reactivity. This reveals that flame behavior shown in Fig. 3 cannot be entirely accounted for by the flame surface area enhancement A_T/A_0, but it should be sought mostly in the enhancement of reactivity given by the synergistic action of turbulence (induced flame curvature and strain) and thermal-diffusive effects within the inner structure of the flame front, as revealed by the behavior of I_0.

The effect of the Ka number at low Lewis numbers is more evident if the stretching factor is compensated with a scaling law of

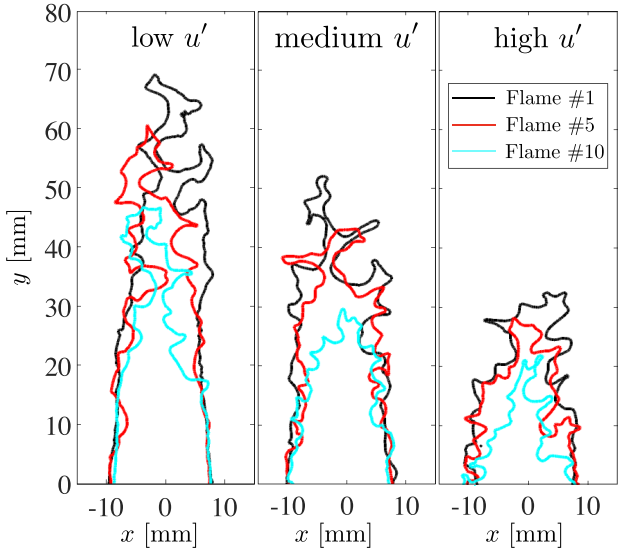

FIG. 4. Instantaneous flame front realizations at different Lewis and Karlovitz numbers. Left, case *low*; middle, case *medium*; right, case *high* (see Table II). Colors: black, flame #1; red, flame #5; cyan, flame #10 (see Table I).

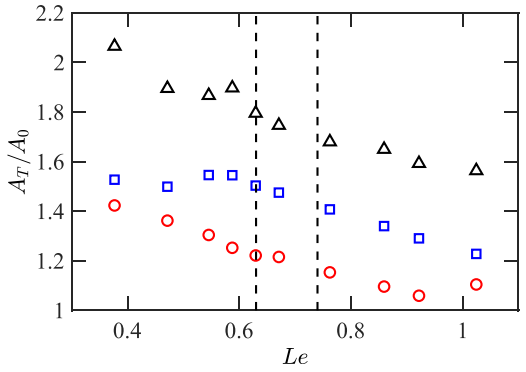

FIG. 5. Behavior of the normalized flame surface area A_T/A_0 for different Lewis numbers and turbulence intensity. Vertical dashed line refers to $Le = 0.63 - 0.74$. For color coding, see Fig. 2.

the kind $Ka^{1/3}$ purposely built for near unity Lewis number (lower panel of Fig. 6) as discussed in Ref. 16, for flames with thermal and mass diffusivity of the same order. In the latter scaling, the discrepancy between turbulent combustion enhancement S_T/S_L^0 and the normalized turbulent area increase A_T/A_0 is entirely accounted for by Karlovitz effects. For Lewis numbers closer to unity, the compensation yields a rather flat response ($I_0 \cdot Ka^{(-1/3)} \simeq const$), but

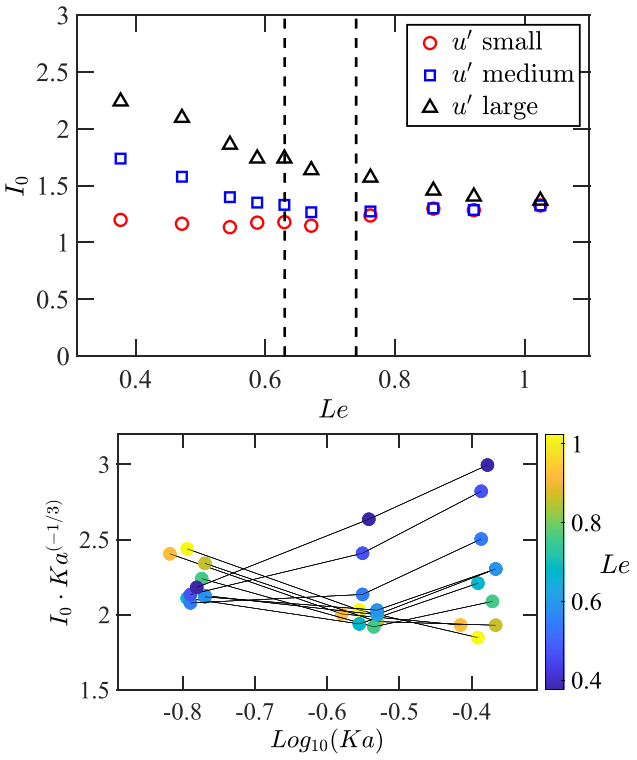

FIG. 6. Top: stretching factor I_0 at different operational conditions. Vertical dashed line refers to $Le = 0.63$–0.74. For color coding, see Fig. 2. Bottom: stretching factor vs Karlovitz number parameterized with Le reported in the color bar. I_0 was compensated with $Ka^{(1/3)}$ according to Ref. 16.

as the Le is further reduced and the thermal diffusivity exceeds the mass diffusivity, the $Ka^{1/3}$ scaling is lost.

B. Parameterization for turbulent flame speed

We now focus on the search for a suitable scaling function for the turbulent flame speed, capable of fitting the experimental results seen thus far. We begin by analyzing its sensitivity to the Karlovitz number.

Concerning the logarithmic plot in Fig. 3 (large symbols), the thermodiffusively unstable regime ($Le < Le_0^*$) is represented by dashed segments whereas the stable regime ($Le > Le_0^*$) with continuous segments, both representing power laws found by linear regressions of the kind of $y = mx + p$. Figure 7 shows that both m and p (in the log–log plot they represent, respectively, the exponent and the prefactor in a power law function) can be well approximated by linear functions of the Karlovitz number. By introducing the ansatz that such parameters are functions of the Karlovitz, Ka, number alone, one may represent the turbulent flame speed as

$$\frac{S_T}{S_L^0}(Ka, Le) = A(Ka) Le^{m(Ka)}, \tag{5}$$

where all the dependencies from the Karlovitz number are explicitly expressed. In this view, the prefactor A stands for turbulent area increase with turbulence, while the power law should mimic the synergistic effect between thermal-diffusive instability and turbulence.

In logarithmic form, this reads

$$Log_{10}\left(\frac{S_T}{S_L^0}\right) = \underbrace{Log_{10}(A)}_{p} + m Log_{10}(Le) \tag{6}$$

with dependencies from Karlovitz and Lewis removed for conciseness and $10^p = A$. Plugging such results into Eq. (5) with $p = \zeta_p(Ka)$ and $m = \zeta_m(Ka)$, we obtain

$$\frac{S_T}{S_L^0}(Ka, Le) = 10^{\zeta_p(Ka)} Le^{\zeta_m(Ka)}, \tag{7}$$

with different values for ζ_p and ζ_m, in the stable (subscript "s") and unstable ("u") regions. Linear regressions of data pictured in Fig. 7 yield exponents $\zeta_p(Ka)$ and $\zeta_m(Ka)$. More precisely, when $Le < Le_0^*$,

$$\begin{aligned} \zeta_{pu}(Ka) &= -0.08 + 0.96 \cdot Ka, \\ \zeta_{mu}(Ka) &= -0.04 - 1.90 \cdot Ka, \end{aligned} \tag{8}$$

and when $Le > Le_0^*$,

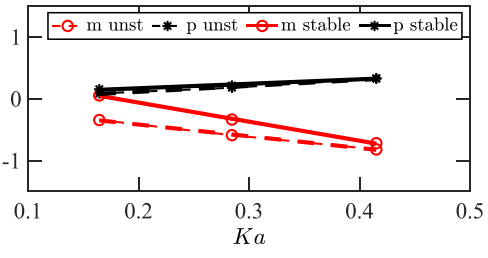

FIG. 7. Fitting parameter of turbulent flame speed power laws of Fig. 3. The fitting function is of the kind $y = mx + p$. Labels *unst* and *stable* refer to regressions for $Le < Le_0^*$ and $Le > Le_0^*$, respectively.

$$\begin{aligned} \zeta_{ps}(Ka) &= 0.03 + 0.72 \cdot Ka, \\ \zeta_{ms}(Ka) &= 0.55 - 3.08 \cdot Ka. \end{aligned} \tag{9}$$

The system of Eqs. (7)–(9) can be used to parameterize the turbulent flame speed at varying Lewis and Karlovitz numbers as shown in Fig. 8, where all the experimental data, belonging to the stable/unstable regions, are well fitted and the critical Lewis number is found at the intersection of the two scaling laws. At high Ka (black triangles), the two curves are almost superimposed, thus supporting once again the hypothesis that turbulence acts to smooth the transition between thermal-diffusive stable/unstable regimes. Indeed, this is also seen by the converging trend of the two angular coefficients m, shown in Fig. 7 and representing the exponent of the scaling law of Eq. (5).

An attempt to find a unifying function to describe the turbulent flame speed being able to model the crossover through the critical Lewis number Le_0^* can be made by introducing the following:

$$\begin{aligned} \frac{S_T}{S_L^0}(Ka, Le)) &= \frac{10^{\zeta_{pu}} \cdot Le^{\zeta_{mu}}}{\left(1 + 10^{\beta} \cdot (Le/Le_0^*)^h\right)^{\gamma/h}}, \\ \beta &= \zeta_{ps} - \zeta_{pu}, \\ \gamma &= \zeta_{mu} - \zeta_{ms}. \end{aligned} \tag{10}$$

When $Le < Le_0^*$, the model behaves as

$$\frac{S_T}{S_L^0}(Ka, Le) \propto 10^{\zeta_{pu}} \cdot Le^{\zeta_{mu}}, \tag{11}$$

and when $Le > Le_0^*$

$$\frac{S_T}{S_L^0}(Ka, Le) \propto 10^{\zeta_{ps}} \cdot Le^{\zeta_{ms}}. \tag{12}$$

In this case, the constant h is used to tune the transition steepness across Le_0^* and a suitable value is taken equal to $h = 5$. The result is plotted in Fig. 9.

To conclude, we compare results obtained with the present parameterization to those obtained with two different models chosen in the literature. The first one is found in Ref. 11 in which the Lewis dependence is set with and exponent of -0.3,

$$\frac{S_T}{S_L^0} = 1.53 \left(\frac{u'}{S_L^0}\right)^{0.55} \left(\frac{\ell_0}{\delta_z}\right)^{0.15} Le^{-0.3}.$$

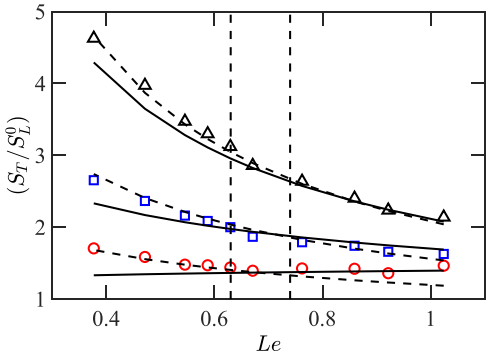

FIG. 8. Turbulent flame speed: experiments vs fitting functions. Dashed lines use parameters defined in Eq. (8). Continuous lines refer to those in Eq. (9).

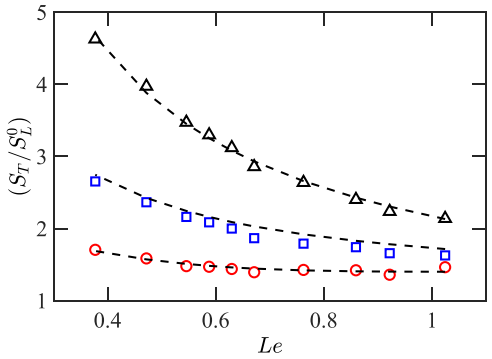

FIG. 9. Turbulent flame speed: experiments vs unified fitting functions of Eq. (10).

The other was originally proposed in Ref. 9 and further modified to take into account the thermal-diffusive effects of the Lewis number,[38]

$$\frac{S_T}{S_L^0} = 1 + \left[0.62 + Le^{-1}\left(\frac{u'}{S_L^0}\right)^{0.75}\left(\frac{\ell_0}{\delta_z}\right)^{0.25} + \left(\frac{1-Le}{Le}\right)\frac{u'/S_L^0}{u'/S_L^0+1}\right],$$

where $\delta_z = \alpha_{T_u}/S_L^0$ is the Zel'dovich flame thickness with α_{T_u} being the unburned gas thermal diffusivity.[35]

Results are plotted in Fig. 10 as a function of the Karlovitz number and parameterized with the Lewis number. With this representation, the synergistic effect at high Karlovitz number is further highlighted. The proposed parameterization (black solid lines), while converging at low *Ka* values, tends to diverge as the turbulence forcing increases and the synergistic effect comes into play. The other two parameterizations reported with green and red dashed lines, instead, apart different amplitudes, in one hand, fail to reproduce the synergistic effect at high Karlovitz, while in the other, do not collapse to a unique value at low level of turbulence.

IV. CONCLUSION

In this work, we have presented an investigation of an experimental dataset under addition of hydrogen in a methane–air Bunsen flame at constant bulk Reynolds number and variable Lewis numbers. These values, for elevated hydrogen volume fractions in the fuel, fall below a critical Lewis number Le_0, indicating that the mixture is thermodiffusively unstable. The turbulent flame speed S_T is monitored at different turbulence intensities and a wide range of Lewis numbers. Results show that S_T/S_L^0 increases as the Lewis number decreases while an enhanced sensitivity to the turbulent velocity fluctuations is observed when the fuel blend is characterized by low *Le*. The increase in turbulent flame speed is shown to be caused by an enhancement of the reactivity of the flame front rather than by the increase in the normalized turbulent flame area. A thorough quantitative parameterization of the experimental results is proposed, based on a functional form depending on both Karlovitz and Lewis numbers, which is also capable of capturing the transition occurring in the *Le* ranges that approach a representative critical Lewis number Le_0^* for the mixture investigated.

While the range of Lewis numbers explored in this work can hardly be enlarged, additional future research efforts are envisaged to span wider variations of the Karlovitz as well as the Reynolds numbers, to assess the validity of the results obtained or establish a more complex behavior of the functional fit proposed for the experimental results.

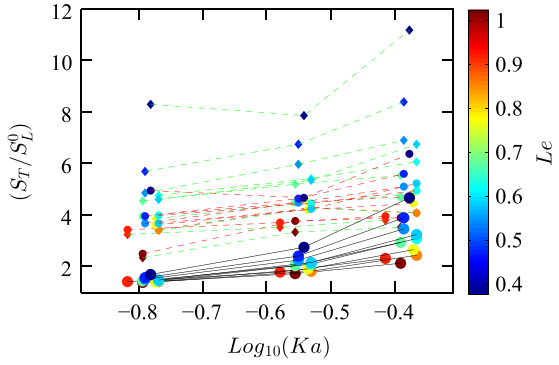

FIG. 10. Turbulent flame speed: experiments vs fitting functions present in literature. Red dashed line,[11] green dashed line,[9,38] and black solid line present fitting function as a function of the Karlovitz number parameterized with the Lewis number. Color code, Lewis number.

ACKNOWLEDGMENTS

This study was performed within the Italian project "RICERCA E SVILUPPO DI TECNOLOGIE PER LA FILIERA DELL'IDROGENO POR-H2" ("Research and Development of Technologies for Hydrogen Chain, POR-H2, WP2, LA2.2.5"), funded by the Italian Ministry of Environment and Energy Security, under the National Recovery and Resilience Plan (PNRR, Mission 2, Component 2, Investment 3.5, project code I83C22001170006). P.E.L acknowledges the support of Sapienza University for the early-stage researchers' funding. F.D. and F.C. acknowledge the support of Baker-Hughes and Lazio Region. This work has been also supported by ICSC (Centro Nazionale di Ricerca in High-Performance Computing, Big Data and Quantum Computing) funded by the European Union—NextGenerationEU.

AUTHOR DECLARATIONS

Conflict of Interest

The authors have no conflicts to disclose.

Author Contributions

Guido Troiani: Conceptualization (equal); Formal analysis (equal); Funding acquisition (equal); Writing – original draft (equal); Writing – review & editing (equal). **Pasquale Eduardo Lapenna:** Conceptualization (equal); Formal analysis (equal); Funding acquisition (equal); Writing – original draft (equal); Writing – review & editing (equal). **Francesco D'Alessio:** Conceptualization (equal); Formal analysis (equal); Funding acquisition (equal); Writing – original draft (equal); Writing – review & editing (equal). **Francesco Creta:** Conceptualization (equal); Formal analysis (equal); Funding acquisition (equal); Writing – original draft (equal); Writing – review & editing (equal).

DATA AVAILABILITY

The data that support the findings of this study are available from the corresponding author upon reasonable request.

APPENDIX: EXPERIMENTAL DATASET OF H_2/CH_4-AIR BUNSEN FLAMES: INTERPLAY OF INTRINSIC INSTABILITIES AND TURBULENCE

Indeed, the choice of $\overline{C} = 0.5$ is somewhat arbitrary when considering the turbulent flame speed as the reactant mass flow rate flowing through an average flame front. The closer the isosurface is chosen to the leading edge of turbulent flame brush, the higher the numerical value of the turbulent flame speed. This is debated in detail in Refs. 48 and 53 where different contributions from literature are considered either evaluated at $\overline{C} = 0.5$ and $\overline{C} = 0.1$, and for the purpose of comparison, they are converted to the value of $\overline{C} = 0.5$.[54] Nonetheless, in Ref. 53 the turbulent flame speeds vs the turbulent intensity evaluated at $\overline{C} = 0.5$ and $\overline{C} = 0.1$ are shown to be described by a power law with the same exponent although with different prefactor, suggesting that the only difference between the two of them is the amplitude but not the general scaling behavior. Also in experimental work[17] and in the review work of Ref. 48, the reference value of $\overline{C} = 0.5$ is chosen for the measurement of the turbulent flame speed.

In the present case, where the Lewis number is lowered to values where the thermodiffusive instabilities are likely present, the choice of the proper isoline value for $\overline{C}$ has its importance. In Fig. 11, the turbulent flame speed of the whole dataset has been evaluated at three different levels of $\overline{C} = [0.1, 0.5, 0.9]$. Results show that at the leading edge of the turbulent flame brush, $\overline{C} = 0.1$, the effects of thermodiffusive instabilities are not evident and, as a result, the turbulent flame speed shows a constant power law across all the Lewis numbers explored. This is also evidenced by the red lines (dashed and solid) in the rightmost column panels expressing the angular coefficients of the linear regressions, which we remind are the exponents of a power law in double logarithmic scale. In addition, from the isoline $\overline{C} = 0.5$ toward the trailing edge of the turbulent flame brush, the general behavior of the results seems not to change. These results seem to imply that the thermodiffusive effects affect the flame mostly in the outer region of the turbulent flame brush, where the small-scale corrugations of the flame front typical of thermodiffusive unstable flames[30] are present. In other words, the fingerlike structures[55] push the most reactive zones of the flame front toward the trailing edge of the turbulent flame brush. This is further strengthened by considering that the ratio between the measure of turbulent area and the average one increases at constant slope with Lewis number, see Fig. 5. This implies that below a critical value of the Lewis number, increase in the turbulent flame speed is not only driven by an area increase but also enhanced by an increase in the reactivity.[27,34,44,56–58]

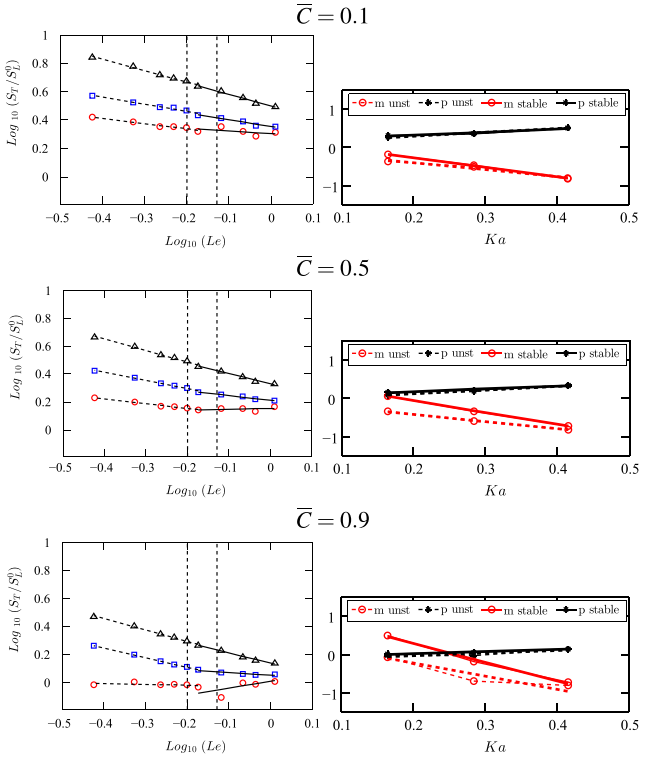

FIG. 11. Left: turbulent flame speed as measured at increasing values of $\overline{C} = [0.1, 0.5, 0.9]$, with the corresponding local linear fitting. Right: Red and black lines, angular coefficient and intercept of local linear fitting, respectively. Dashed lines, thermodiffusively unstable flames (corresponding to leftmost points in the panels of the first column); solid lines, thermodiffusively stable flames (corresponding to rightmost points in the panels of the first column).

REFERENCES

[1] G. Damköhler, "Der Einfluss der Turbulenz auf die Flammengeschwindigkeit in Gasgemischen," Z. Elektrochem. Angew. Phys. Chem. **46**, 601 (1940).
[2] R. Abdel-Gayed, D. Bradley, M. Hamid, and M. Lawes, "Lewis number effects on turbulent burning velocity," Symp. Int. Combust. **20**, 505–512 (1985).
[3] D. Haworth and T. Poinsot, "Numerical simulations of Lewis number effects in turbulent premixed flames," J. Fluid Mech. **244**, 405 (1992).
[4] C. K. Law and O. Kwon, "Effects of hydrocarbon substitution on atmospheric hydrogen–air flame propagation," Int. J. Hydrogen Energy **29**, 867 (2004).
[5] S. R. Muppala, N. K. Aluri, F. Dinkelacker, and A. Leipertz, "Development of an algebraic reaction rate closure for the numerical calculation of turbulent premixed methane, ethylene, and propane/air flames for pressures up to 1.0 MPa," Combust. Flame **140**, 257 (2005).
[6] A. N. Lipatnikov, Y.-R. Chen, and S. Shy, "An experimental study of the influence of Lewis number on turbulent flame speed at different pressures," Proc. Combust. Inst. **39**, 2339 (2023).
[7] H. Kolla, J. Rogerson, N. Chakraborty, and N. Swaminathan, "Scalar dissipation rate modeling and its validation," Combust. Sci. Technol. **181**, 518 (2009).
[8] N. Peters, "The turbulent burning velocity for large-scale and small-scale turbulence," J. Fluid Mech. **384**, 107 (1999).
[9] Ö. L. Gülder, "Turbulent premixed flame propagation models for different combustion regimes," Symp. Int. Combust. **23**, 743–750 (1991).
[10] V. L. Zimont, "Gas premixed combustion at high turbulence. Turbulent flame closure combustion model," Exp. Thermal Fluid Sci. **21**, 179 (2000).
[11] D. Bradley, "How fast can we burn?," Symp. Int. Combust. **24**, 247–262 (1992).
[12] J. B. Bell, M. S. Day, and J. F. Grcar, "Numerical simulation of premixed turbulent methane combustion," Proc. Combust. Inst. **29**, 1987 (2002).
[13] E. R. Hawkes and J. H. Chen, "Comparison of direct numerical simulation of lean premixed methane–air flames with strained laminar flame calculations," Combust. Flame **144**, 112 (2006).
[14] G. Troiani, F. Battista, and F. Picano, "Turbulent consumption speed via local dilatation rate measurements in a premixed bunsen jet," Combust. Flame **160**, 2029 (2013).
[15] P. E. Lapenna, G. Troiani, R. Lamioni, and F. Creta, "Mitigation of Darrieus–Landau instability effects on turbulent premixed flames," Proc. Combust. Inst. **38**, 2885 (2021a).

[16]G. Nivarti, R. Cant, and S. Hochgreb, "Reconciling turbulent burning velocity with flame surface area in small-scale turbulence," J. Fluid Mech. **858**, R1 (2019).
[17]T. M. Wabel, A. W. Skiba, and J. F. Driscoll, "Turbulent burning velocity measurements: Extended to extreme levels of turbulence," Proc. Combust. Inst. **36**, 1801 (2017).
[18]F. T. Yuen and Ö. L. Gülder, "Turbulent premixed flame front dynamics and implications for limits of flamelet hypothesis," Proc. Combust. Inst. **34**, 1393 (2013).
[19]M. Matalon and B. J. Matkowsky, "Flames as gasdynamic discontinuities," J. Fluid Mech. **124**, 239 (1982).
[20]P. Clavin and F. Williams, "Effects of molecular diffusion and of thermal expansion on the structure and dynamics of premixed flames in turbulent flows of large scale and low intensity," J. Fluid Mech. **116**, 251 (1982).
[21]E. Al Sarraf, C. Almarcha, J. Quinard, B. Radisson, B. Denet, and P. Garcia-Ybarra, "Darrieus–Landau instability and Markstein numbers of premixed flames in a Hele-Shaw cell," Proc. Combust. Inst. **37**, 1783 (2019).
[22]C. E. Frouzakis, N. Fogla, A. G. Tomboulides, C. Altantzis, and M. Matalon, "Numerical study of unstable hydrogen/air flames: shape and propagation speed," Proc. Combust. Inst. **35**, 1087 (2015).
[23]L. Berger, M. Grinberg, B. Jürgens, P. E. Lapenna, F. Creta, A. Attili, and H. Pitsch, "Flame fingers and interactions of hydrodynamic and thermodiffusive instabilities in laminar lean hydrogen flames," Proc. Combust. Inst. **39**, 1525 (2023).
[24]F. Creta, R. Lamioni, P. E. Lapenna, and G. Troiani, "Interplay of Darrieus-Landau instability and weak turbulence in premixed flame propagation," Phys. Rev. E **94**, 53102 (2016).
[25]P. E. Lapenna, R. Lamioni, G. Troiani, and F. Creta, "Large scale effects in weakly turbulent premixed flames," Proc. Combust. Inst. **37**, 1945 (2019).
[26]G. Troiani, F. Creta, and M. Matalon, "Experimental investigation of Darrieus–Landau instability effects on turbulent premixed flames," Proc. Combust. Inst. **35**, 1451 (2015).
[27]G. Rocco, F. Battista, F. Picano, G. Troiani, and C. M. Casciola, "Curvature effects in turbulent premixed flames of H_2/air: A DNS study with reduced chemistry," Flow, Turbul. Combust. **94**, 359 (2015).
[28]S. Yang, A. Saha, Z. Liu, and C. K. Law, "Role of Darrieus–Landau instability in propagation of expanding turbulent flames," J. Fluid Mech. **850**, 784 (2018).
[29]G. Troiani, P. Lapenna, R. Lamioni, and F. Creta, "Self-wrinkling induced by Darrieus-Landau instability in turbulent premixed Bunsen flames from low to moderately high Reynolds numbers," Phys. Rev. Fluids **7**, 53202 (2022).
[30]F. Creta, P. E. Lapenna, R. Lamioni, N. Fogla, and M. Matalon, "Propagation of premixed flames in the presence of Darrieus–Landau and thermal diffusive instabilities," Combust. Flame **216**, 256 (2020).
[31]L. Berger, A. Attili, and H. Pitsch, "Synergistic interactions of thermodiffusive instabilities and turbulence in lean hydrogen flames," Combust. Flame **244**, 112254 (2022a).
[32]G. Troiani, P. E. Lapenna, F. D'Alessio, and F. Creta, in *11th European Combustion Meeting* (ECM, 2023), pp. 1320–1325.
[33]P. E. Lapenna, G. Troiani, F. D'Alessio, and F. Creta, "Synergistic interplay of thermodiffusive instability and turbulence in premixed flames," Proc. Combust. Inst. **40**, 105499 (2024).
[34]O. Chaib, S. Hochgreb, and I. Boxx, "An experimental marker of thermodiffusive instability in hydrogen-enriched flames," Proc. Combust. Inst. **40**, 105763 (2024).
[35]J. Bechtold and M. Matalon, "The dependence of the Markstein length on stoichiometry," Combust. Flame **127**, 1906 (2001).
[36]E. Hu, Z. Huang, J. He, C. Jin, and J. Zheng, "Experimental and numerical study on laminar burning characteristics of premixed methane–hydrogen–air flames," Int. J. Hydrogen Energy **34**, 4876 (2009).
[37]C. K. Law, *Combustion Physics* (Cambridge University Press, 2010).
[38]V. Mohan, M. Herbert, M. Klein, and N. Chakraborty, "A direct numerical simulation assessment of turbulent burning velocity parametrizations for non-unity Lewis numbers," Energies **16**, 2590 (2023).
[39]N. Bouvet, F. Halter, C. Chauveau, and Y. Yoon, "On the effective Lewis number formulations for lean hydrogen/hydrocarbon/air mixtures," Int. J. Hydrogen Energy **38**, 5949 (2013).
[40]D. G. Goodwin, H. K. Moffat, I. Schoegl, R. L. Speth, and B. W. Weber, "Cantera: An object-oriented software toolkit for chemical kinetics, thermodynamics, and transport processes" (2022). https://www.cantera.org version 2.6.0.
[41]T. Aizawa, "Diode-laser wavelength-modulation absorption spectroscopy for quantitative in situ measurements of temperature and OH radical concentration in combustion gases," Appl. Opt. **40**, 4894 (2001).
[42]L. Berger, A. Attili, and H. Pitsch, "Intrinsic instabilities in premixed hydrogen flames: Parametric variation of pressure, equivalence ratio, and temperature. part 1-dispersion relations in the linear regime," Combust. Flame **240**, 111935 (2022).
[43]M. Matalon, C. Cui, and J. Bechtold, "Hydrodynamic theory of premixed flames: effects of stoichiometry, variable transport coefficients and arbitrary reaction orders," J. Fluid Mech. **487**, 179 (2003).
[44]T. Howarth and A. Aspden, "An empirical characteristic scaling model for freely-propagating lean premixed hydrogen flames," Combust. Flame **237**, 111805 (2022).
[45]P. E. Lapenna, R. Lamioni, and F. Creta, "Subgrid modeling of intrinsic instabilities in premixed flame propagation," Proc. Combust. Inst. **38**, 2001 (2021).
[46]R. Lamioni, P. E. Lapenna, G. Troiani, and F. Creta, "Strain rates, flow patterns and flame surface densities in hydrodynamically unstable, weakly turbulent premixed flames," Proc. Combust. Inst. **37**, 1815 (2019).
[47]G. Troiani and M. Marrocco, "Fractal Analysis of Fluorescence Images to Assess Robustness of Reference-surface Positioning in Flame Fronts," Combust. Sci. Technol. **193**, 1782 (2021).
[48]J. F. Driscoll, "Turbulent premixed combustion: Flamelet structure and its effect on turbulent burning velocities," Prog. Energy Combust. Sci. **34**, 91 (2008).
[49]E. R. Hawkes and J. H. Chen, "Direct numerical simulation of hydrogen-enriched lean premixed methane–air flames," Combust. Flame **138**, 242 (2004).
[50]L. Berger, A. Attili, M. Gauding, and H. Pitsch, "Effects of Karlovitz number variations on thermodiffusive instabilities in lean turbulent hydrogen jet flames," Proc. Combust. Inst. **40**, 105219 (2024).
[51]C. K. Law, G. Jomaas, and J. K. Bechtold, "Cellular instabilities of expanding hydrogen/propane spherical flames at elevated pressures: Theory and experiment," Proc. Combust. Inst. **30**, 159 (2005).
[52]H.-Y. Hsieh, S. M. Mousavi, A. N. Lipatnikov, and S. S. Shy, "Experimental study of the influence of Lewis number, laminar flame thickness, temperature, and pressure on turbulent flame speed using hydrogen and methane fuels," Proc. Combust. Inst. **40**, 105752 (2024).
[53]L. Jiang, S. Shy, W. Li, H. Huang, and M. Nguyen, "High-temperature, high-pressure burning velocities of expanding turbulent premixed flames and their comparison with Bunsen-type flames," Combust. Flame **172**, 173 (2016).
[54]D. Bradley, M. Lawes, and M. Mansour, "Correlation of turbulent burning velocities of ethanol–air, measured in a fan-stirred bomb up to 1.2MPa," Combust. Flame **158**, 123 (2011).
[55]L. Berger, K. Kleinheinz, A. Attili, and H. Pitsch, "Characteristic patterns of thermodiffusively unstable premixed lean hydrogen flames," Proc. Combust. Inst. **37**, 1879 (2019).
[56]A. Aspden, M. Day, and J. Bell, "Characterization of low Lewis number flames," Proc. Combust. Inst. **33**, 1463 (2011).
[57]T. Howarth, E. Hunt, and A. Aspden, "Thermodiffusively-unstable lean premixed hydrogen flames: Phenomenology, empirical modelling, and thermal leading points," Combust. Flame **253**, 112811 (2023).
[58]H. Lee, B. Wu, P. Dai, M. Wan, and A. N. Lipatnikov, "Area increase and stretch factor in lean hydrogen-air turbulent flames," Proc. Combust. Inst. **40**, 105687 (2024).